Research Article | Vol. 30, No. 22 / 24 Oct 2022 / Optics Express 40101

Optics EXPRESS

Influence of birefringence- and core ellipticity-induced mode coupling on the gain statistics of forward-pumped Raman amplified few-mode fiber links

GIANLUCA MARCON,[1] ANDREA GALTAROSSA,[1,2] LUCA PALMIERI,[1,2] AND MARCO SANTAGIUSTINA[1,2,*]

[1]Department of Information Engineering, University of Padua, Padova, Italy
[2]National Inter-University Consortium for Telecommunications (CNIT), Pisa, Italy
[*]marco.santagiustina@unipd.it

Abstract: The equations describing light propagation in a few-mode fiber for space-division multiplexing are derived under the presence of linear mode coupling and both Kerr- and Raman-induced nonlinearity. By considering physical models of stress birefringence and core ellipticity, the effect of such fiber imperfections on the gain of a forward-pumped Raman-amplified link is assessed through numerical simulations. The average gain and the variation of signal power at the output of the amplified fiber span is numerically evaluated for different levels of coupling strength in fibers supporting 2 and 4 groups of LP modes, identifying three main propagation regimes and assessing the effect of coupling between different groups of degenerate modes.

1. Introduction

Although Spatial Division Multiplexing (SDM) has emerged as the solution to overcome the nonlinear Shannon limit of Single Mode Fibers (SMFs) through the lower power-density enabled by physically separating multiple information streams, nonlinear effects remain the ultimate factor determining the maximum achievable capacity of optical fiber communications [1]. The modeling of such effects is then of paramount importance in the understanding of propagation limits in both Few Mode Fibers (FMFs) and Multi-Core Fibers (MCFs), especially in the presence of mode coupling.

In principle, the interaction between all possible combinations of modes/cores and wavelengths must be studied to completely describe the nonlinear phenomena occurring in SDM transmissions. The most general description of such interaction in Multi-Mode fibers (MMFs) is given by the Multimode Nonlinear Schrödinger Equation (MM-NLSE), in which linear mode coupling is neglected and the Kerr interaction is described by a set of $(2N)^4$ coefficients between the mode functions, where N is the total number of spatial modes, and the factor 2 accounts for polarization degeneracy [2,3].

In the regime of strong mode coupling, it is argued that the linear mode mixing effects occur on length scales much shorter than the nonlinear interaction length [4]. These considerations justify the simplification of the equations obtained by averaging the overlap integrals appearing in the MM-NLSE, resulting in the generalized Manakov equation, which extends the well-known Manakov-PMD equation used in the study of polarization coupling in SMFs [4,5]. An equivalent equation has also been derived in Ref. [6] and extended to the case of MCFs. A further version of the generalized Manakov equation is obtained when considering strong coupling occurring only between modes belonging to the same group of quasi-degenerate modes of a FMF, with no interaction occurring between different groups. In this case, the propagation of the mode groups is described by the coupled multi component Manakov equations, extending the results of Ref.

#459381 https://doi.org/10.1364/OE.459381
Journal © 2022 Received 27 Mar 2022; revised 3 Jul 2022; accepted 6 Jul 2022; published 14 Oct 2022

Optics EXPRESS

[4] by separating the intra-group and inter-group nonlinear effects with two separate averaged nonlinear coefficients [7].

The models previously introduced generally described the coupling process through a fully stochastic approach for mathematical convenience, without considering the different physical mechanisms which cause the coupling process, such as the ellipticity of the fiber core, birefringence, twisting, or bending, as modeled in [8,9]. In Ref. [10] such physical models were included in the study of Four-Wave Mixing (FWM) in FMFs, demonstrating a reduction in FWM efficiency when linear mode coupling is considered.

For the case of Raman amplification, Ref. [11] extended the coupled multi component Manakov equations with terms describing the Raman interaction, under the hypothesis of strong coupling between degenerate modes of the same group, and total absence of linear coupling between different groups; this model is at the base of most of the published numerical results in the context of FMF Raman amplification [12–15].

However, numerical results showing the effects of mode coupling on Raman amplification are lacking, regardless of the regime of coupling considered, with the only contribution considering Raman scattering effects in the context of Raman induced crosstalk between different channels of a Wavelength Division Multiplexing (WDM) transmission [16].

In this article, following Ref. [17], which presented a model for SMF Raman amplifiers with Polarization Mode Dispersion (PMD) effects, a set continuous-wave equations is derived, describing the evolution of the modes at two different wavelengths, a pump and a signal of a Raman amplifier, modeling linear coupling based on the underlying physical phenomena. Through numerical integration of the equations, the combined effect of stress birefringence and core ellipticity on the gain statistics of a forward-pumped FMF Raman amplifier is studied over an ensemble of thousands of fiber realizations for different coupling conditions on two step-index fibers supporting 2 and 4 groups of degenerate Linearly Polarized (LP) modes, respectively.

2. Analytical model

The equations that have been derived in this article describe the evolution of the complex amplitude of the modes at two different frequencies ω_ℓ and ω_f, which correspond to the Raman pump and the information signal, hereinafter the pump and the signal.

The model considers light propagation in the continuous wave (CW) regime undergoing both linear and nonlinear mode coupling, with the former stemming from imperfections of the fiber profile, and the latter caused by Kerr and Raman effects. The complex amplitude of the M_ℓ (M_f) spatial modes at frequency ω_ℓ (ω_f) are modeled with the following set of coupled nonlinear differential equations

Optics EXPRESS

$$
\begin{aligned}
\frac{\partial a_{\ell\nu}}{\partial z} = &-\frac{\alpha_\ell}{2} a_{\ell\nu} + j\beta_{\ell\nu} a_{\ell\nu} + j \sum_{\mu=1}^{2M_\ell} K_{\nu\mu}(\omega_\ell) a_{\ell\mu} \\
&+ \frac{j\omega_\ell}{4} \frac{\epsilon_0}{8} [\sigma + 2\tilde{b}_0] \sum_{\mu=1}^{2M_\ell} \sum_{\eta=1}^{2M_\ell} \sum_{\rho=1}^{2M_\ell} Q^{(1)}_{\nu\rho\mu\eta} a_{\ell\mu} a_{\ell\eta} a^*_{\ell\rho} \\
&+ \frac{j\omega_\ell}{4} \frac{\epsilon_0}{4} [\sigma + 2\tilde{a}_0 + \tilde{b}_0] \sum_{\mu=1}^{2M_\ell} \sum_{\eta=1}^{2M_\ell} \sum_{\rho=1}^{2M_\ell} Q^{(2)}_{\nu\rho\mu\eta}(\omega_\ell) a^*_{\ell\mu} a_{\ell\eta} a_{\ell\rho} \\
&+ \frac{j\omega_\ell}{4} \frac{\epsilon_0}{4} [\sigma + 2\tilde{a}_0 + \tilde{b}_\Omega] \sum_{\mu=1}^{2M_f} \sum_{\eta=1}^{2M_f} \sum_{\rho=1}^{2M_\ell} Q^{(3)}_{\nu\rho\mu\eta}(\omega_\ell) a^*_{f\mu} a_{f\eta} a_{\ell\rho} \\
&+ \frac{j\omega_\ell}{4} \frac{\epsilon_0}{4} [\sigma + \tilde{b}_0 + \tilde{b}_\Omega] \sum_{\mu=1}^{2M_f} \sum_{\eta=1}^{2M_\ell} \sum_{\rho=1}^{2M_f} Q^{(4)}_{\nu\rho\mu\eta}(\omega_\ell) a_{f\mu} a_{\ell\eta} a^*_{f\rho} \\
&+ \frac{j\omega_\ell}{4} \frac{\epsilon_0}{4} [\sigma + 2\tilde{a}_\Omega + \tilde{b}_0] \sum_{\mu=1}^{2M_f} \sum_{\eta=1}^{2M_\ell} \sum_{\rho=1}^{2M_f} Q^{(5)}_{\nu\rho\mu\eta}(\omega_\ell) a^*_{f\mu} a_{\ell\eta} a_{f\rho},
\end{aligned}
\tag{1}
$$

where α_ℓ is the fiber loss coefficient, $\beta_{\ell\nu}$ is the propagation constant of the νth mode at frequency ω_ℓ, $\Omega = \omega_\ell - \omega_f$, σ is a parameter describing the Kerr effect, while $\tilde{a}_\omega$ and $\tilde{b}_\omega$ are the parallel and cross-polarized delayed Raman response functions evaluated at the detuning frequency ω [17].

The expression of linear coupling coefficients $K_{\nu\mu}$ for frequency ω_ℓ is that obtained using coupled-mode theory [18,19]

$$
K_{\nu\mu}(\omega_\ell) = \epsilon_0 \frac{\omega_\ell}{4} \iint_{-\infty}^{+\infty} \mathbf{F}^\dagger_{\ell\nu} \Delta\tilde{\boldsymbol{\epsilon}}_\ell \mathbf{F}_{\ell\mu} \, \mathrm{d}x\mathrm{d}y, \tag{2}
$$

where $\mathbf{F}_{\ell\mu}$ is the electric field distribution function of the μth fiber mode at frequency ω_ℓ. The nature of the underlying process causing linear mode coupling is described through the dielectric tensor perturbation $\Delta\tilde{\boldsymbol{\epsilon}}_\ell$. Several models for different kinds of physical effects causing the coupling between modes are present in the literature; a summary of the most relevant cases and their effect on the coupling of LP modes is given in Refs. [8,9], while the study of birefringence and core ellipticity is carried out in Ref. [19] for the case of air-core fibers supporting Orbital-Angular-Momentum (OAM) modes, and in [10] for FWM in WDM systems.

The terms accounting for the nonlinear interaction between modes are determined by a set of overlap integrals $Q_{\nu\rho\mu\eta}$ involving the combination of 4 different modes. Their expression is reported in Table 1. Further details about the derivation of the presented equations are given in the Appendix.

Optics EXPRESS

Table 1. Expression of the overlap integrals that define the strength of the nonlinear interaction between modes.

$Q^{(1)}_{\nu\rho\mu\eta}(\omega_\ell) = \iint_{-\infty}^{+\infty} (\mathbf{F}^*_{\ell\nu} \cdot \mathbf{F}^*_{\ell\rho})(\mathbf{F}_{\ell\mu} \cdot \mathbf{F}_{\ell\eta})\,\mathrm{d}x\mathrm{d}y$
$Q^{(2)}_{\nu\rho\mu\eta}(\omega_\ell) = \iint_{-\infty}^{+\infty} (\mathbf{F}^*_{\ell\nu} \cdot \mathbf{F}_{\ell\rho})(\mathbf{F}^*_{\ell\mu} \cdot \mathbf{F}_{\ell\eta})\,\mathrm{d}x\mathrm{d}y$
$Q^{(3)}_{\nu\rho\mu\eta}(\omega_\ell) = \iint_{-\infty}^{+\infty} (\mathbf{F}^*_{\ell\nu} \cdot \mathbf{F}_{\ell\rho})(\mathbf{F}^*_{f\mu} \cdot \mathbf{F}_{f\eta})\,\mathrm{d}x\mathrm{d}y$
$Q^{(4)}_{\nu\rho\mu\eta}(\omega_\ell) = \iint_{-\infty}^{+\infty} (\mathbf{F}^*_{\ell\nu} \cdot \mathbf{F}^*_{f\rho})(\mathbf{F}_{f\mu} \cdot \mathbf{F}_{\ell\eta})\,\mathrm{d}x\mathrm{d}y$
$Q^{(5)}_{\nu\rho\mu\eta}(\omega_\ell) = \iint_{-\infty}^{+\infty} (\mathbf{F}^*_{\ell\nu} \cdot \mathbf{F}_{f\rho})(\mathbf{F}^*_{f\mu} \cdot \mathbf{F}_{\ell\eta})\,\mathrm{d}x\mathrm{d}y$

3. Numerical methods

As introduced in the previous section, the linear effects occurring during propagation in a FMF are accounted for by the linear terms of Eq. (1), which can be written in matrix form describing the evolution of the vector of complex amplitudes of the propagating modes $\mathbf{a}$ as

$$\frac{\partial \mathbf{a}}{\partial z} = -\frac{\alpha}{2}\mathbf{a} + j(\mathbf{B} + \mathbf{K})\mathbf{a}, \tag{3}$$

which is the same used in Refs. [8,19] with the addition of fiber losses.

For simplicity, we momentarily drop the subscript notation to indicate the frequency dependence of each quantity, as the linear effects can be treated separately for each frequency component.

The local coupling effects, caused by perturbations, are described by the coupling matrix $\mathbf{K}$ whose coefficients are determined by the overlap integrals in Eq. (2), while $\mathbf{B}$ is the diagonal matrix of propagation constants. The coupling strength of a specific perturbation can be calculated from the eigenvalues κ_i of the coupling matrix and related to the coupling beat length L_κ by

$$L_\kappa = \frac{2\pi}{\Delta\kappa}, \tag{4}$$

where $\Delta\kappa = \max_i \kappa_i - \min_i \kappa_i$ is the coupling strength.

In the most general case, both the strength and the orientation of the various perturbations can vary randomly along the fiber. It is then necessary to account for the dependence of the coupling matrix on the position along the fiber. If we call $\bar{\mathbf{K}}$ the normalized coupling matrices (i.e. with unit coupling strength and computed with the reference perturbation aligned to the reference frame of the fiber) then the coupling matrix at position z due to various perturbations (indexed by ζ) reads [19]

$$\mathbf{K}(z) = \sum_\zeta \Gamma_\zeta(z)\mathbf{R}(\theta_\zeta(z))\bar{\mathbf{K}}^{(\zeta)}\mathbf{R}^\top(\theta_\zeta(z)), \tag{5}$$

where $\Gamma_\zeta(z)$ and $\theta_\zeta(z)$ are the strength and angle of perturbation ζ, respectively, and $\mathbf{R}$ is a unitary rotation matrix. The form of matrix $\mathbf{R}$ is that of a block diagonal matrix, where each block corresponds to a different group of degenerate modes [9]. Hereinafter, in each group of degenerate modes, we order the modes by alternating x and y polarizations of the even degeneracy, and then the x and y polarizations of odd degeneracy.

Here, as in Ref. [19], we focus only on the effect of stress birefringence and core ellipticity, which are perturbations that are closely related, as they are mainly due to the fiber manufacturing process. In particular, we assume that they act on the fiber with the same perturbation angle, and contribute equally to the overall strength [20,21]. The total coupling matrix for this case can be

Optics EXPRESS

written as

$$\mathbf{K}(z) = \Gamma(z)\mathbf{R}(\theta(z))\bar{\mathbf{K}}^{(t)}\mathbf{R}^{\top}(\theta(z)), \tag{6}$$

where $\mathbf{K}^{(t)} = \bar{\mathbf{K}}^{(e)} + \bar{\mathbf{K}}^{(b)}$, is the total, unnormalized coupling matrix, while $\bar{\mathbf{K}}^{(e)}$ and $\bar{\mathbf{K}}^{(b)}$ are the normalized coupling matrices for core ellipticity and stress birefringence, respectively.

In order to model the evolution of these perturbations along the fiber, we use the Fixed-Modulus Model (FMM), also used in the study PMD in SMFs [22]. According to FMM, the strength of the perturbation remains constant along the fiber, while its orientation angle θ varies according to a Wiener process [22]

$$\frac{d\theta}{dz} = -\sigma_\theta w(z), \tag{7}$$

where w is a Gaussian process with zero mean and unit variance, and σ_θ is related to the correlation length L_c of the process [22]

$$\sigma_\theta = \frac{1}{\sqrt{2L_c}}. \tag{8}$$

We can set the strength of the total perturbation, or equivalently, the coupling beat length, by simply multiplying the total normalized matrix $\bar{\mathbf{K}}^{(t)}$ by a scalar factor. Under the FMM hypothesis, this translates to setting

$$\Gamma(z) = \Gamma_0 = \frac{2\pi}{L_\kappa}. \tag{9}$$

To numerically model the evolution of the perturbations along the fiber, the Wiener process is discretized by dividing the optical fiber in a cascade of N_s plates, each of size $\delta z = L/N_s$, where L is the total length of the fiber [19,23,24]. The number of plates must be sufficiently high so that the angle $\theta(z)$ can be considered almost constant over the plate length, meaning that $\delta z \ll L_c$.

Over the length of the kth plate, the propagation equation then assumes the following form

$$\frac{\partial \mathbf{a}}{\partial z} = \mathbf{L}(\theta_k)\mathbf{a} \qquad z \in [k\delta z, (k+1)\delta z], \tag{10}$$

with

$$\mathbf{L}(\theta_k) = -\frac{\alpha}{2} + j\left[\mathbf{B} + \frac{2\pi}{L_\kappa}\mathbf{R}(\theta_k)\bar{\mathbf{K}}^{(t)}\mathbf{R}^{\top}(\theta_k)\right]. \tag{11}$$

Eq. (10) has a closed form solution written as

$$\mathbf{a}(k+1) = \exp[\mathbf{L}(\theta_k)\delta z]\mathbf{a}(k). \tag{12}$$

This fact brings a significant advantage when dealing with the numerical solution of the linear part of Eq. (1): if this were not the case, we would need to apply conventional integration schemes with a step size that is substantially smaller than the modal beat length of the fiber, which depends on the difference between the propagation constants of the fiber modes, resulting in integration steps of fractions of millimeters. Instead, the step size required to accurately follow the evolution of the vector of complex amplitudes could only be a fraction of the correlation length of the Wiener process describing the orientation of the perturbation, which is usually in the order of tens of meters.

An exact solution cannot be determined when both linear and nonlinear effects act together. The typical approach in such cases is to employ the split-step integration schemes [25]. In the first step, linear propagation is solved using the previously presented approach; in the second step, the nonlinear operator is applied on the linearly propagated field computed in the first step using a fourth-order Runge-Kutta scheme.

The length scale of nonlinear effects is typically much longer than that of linear effects [6,23,26], so we can safely use the same step size employed for the linear propagation.

Optics EXPRESS

4. Results

We consider a few-mode fiber Raman amplified link in which only CW pump and signal are propagating. The signal frequency corresponds to the wavelength $\lambda_s = 1550$ nm, while the pump is frequency up shifted by 12 THz.

We simulate two different FMFs, supporting 2 (LP_{01} and LP_{11}) and 4 (LP_{01}, LP_{11}, LP_{21}, and LP_{02}) groups of LP modes, respectively. Both fibers have a cladding diameter $d_{cl} = 120$ μm and a core diameter $d_{co} = 12$ μm, and are characterized by a step-index profile. The core refractive index n_{co} and cladding refractive index n_{cl} are calculated by a commercial Finite Element Method (FEM) solver to guarantee that the number of supported modes at the signal and pump frequencies is the same, while also ensuring that we are operating far from the cutoff-frequency of the higher-order modes. With these considerations, $n_{co} = 1.4674$ for both fibers, while $n_{cl} = 1.46$ for 2-mode fiber and $n_{cl} = 1.4545$ for the 4-mode fiber.

The two fiber geometries have been simulated using the FEM solver to compute the propagation constant and the field distribution of each guided mode. As the calculated modes are actually hybrid modes, a standard combination procedure is applied to convert them to LP modes [27]. Moreover, an orthogonalization step is also applied to align the modes to the Cartesian reference frame. After normalizing the amplitude of the mode distribution functions (see Eq. (29) in the Appendix), the integrals in Eq. (2) and Table 1 are numerically evaluated at both signal and pump frequencies to obtain the linear and nonlinear coupling coefficients, respectively.

4.1. Linear coupling matrices

In this article the effects of stress birefringence and core ellipticity are included by properly modeling the tensor of dielectric perturbation $\Delta\tilde{\epsilon}$ of Eq. (2) [8]. Depending on the form of the tensor, coupling between different modes can occur either among transverse components of the field, resulting in a strong interaction, or between longitudinal components, causing weaker effects.

Stress birefringence, which is quantified by the difference in refractive index δn between fast and slow axis of the fiber, is responsible for the detuning of the x- and y- polarization of each spatial mode [8,9]. Due to orthogonality conditions, coupling only occurs between transverse components of the modes belonging to the same group [9].

The case of an elliptical core is instead described by a parameter (γ), which represents the overall ellipticity of the fiber core in terms of maximum radius variation [8,9].

As detailed in Ref. [9], core ellipticity causes coupling between the transverse components of modes with azimuthal order 1 and of modes whose azimuthal order differs by 2. Coupling between longitudinal components instead occurs among modes with the same azimuthal order or with orders differing by 4. This means that in a fiber supporting only the LP_{01} and LP_{11} groups, no inter-group coupling occurs. Differently, if the fiber also supports the propagation of the LP_{21} and LP_{02} groups, strong inter-group coupling is expected for the LP_{01}-LP_{21} and LP_{02}-LP_{21} pairs, while weak inter-group coupling is predicted between the LP_{01} and LP_{02} groups.

From the theoretical formulation of the perturbation tensor, the linear coupling integrals of Eq. (2) are numerically evaluated at both the pump and the signal frequency, using reference values of birefringence $\bar{\delta n}$ and ellipticity $\bar{\gamma}$.

Some post-processing steps have also been performed in order to remove spurious interaction between uncoupled modes:

1. the coupling coefficients must be real for both birefringence and core ellipticity, so the residual imaginary part of the corresponding matrices is set to 0;

2. due to Eq. (34), Hermitian symmetry is imposed;

Optics EXPRESS

3. Finally, to normalize the matrices, they are scaled by the difference between their biggest and smallest eigenvalues, i.e. their coupling strength. As the perturbation strength depends linearly on δn and γ, the reference birefringence and ellipticity values can be scaled by the same amount.

The absolute value of the resulting coefficients of the linear coupling matrices for the 2-modes (4-modes) fiber are reported in logarithmic scale in Fig. 1 (Fig. 2).

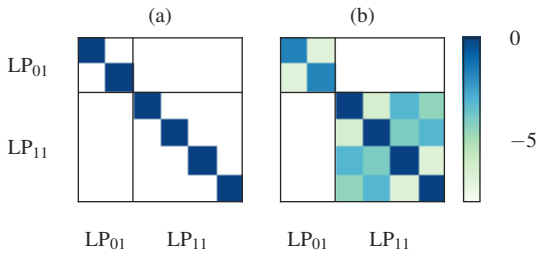

Fig. 1. (a) Stress birefringence and (b) core ellipticity coupling matrices for the 2-modes fiber. Values are normalized and reported in logarithmic scale.

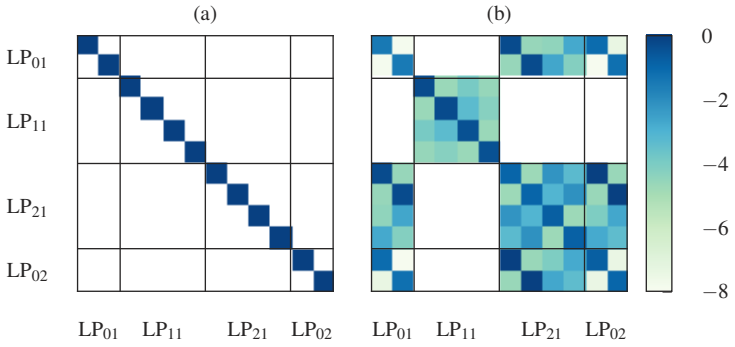

Fig. 2. (a) Stress birefringence and (b) core ellipticity coupling matrices for the 4-modes fiber. Values are normalized and reported in logarithmic scale.

Once the normalized matrices $\bar{\mathbf{K}}^{(e)}$ and $\bar{\mathbf{K}}^{(b)}$ are obtained, along with their reference birefringence $\bar{\delta n}$ and ellipticity $\bar{\gamma}$, the total normalized linear coupling matrix $\bar{\mathbf{K}}^{(t)}$ is obtained by adding the two matrices and normalizing it by its coupling strength.

This matrix is computed only once for each frequency, and scaled accordingly during simulation to obtain the desired total coupling strength $\Delta\kappa$ (or equivalently the beat length L_κ). The corresponding birefringence and ellipticity parameters are retrieved using the approximation

$$\Delta\kappa \approx \Delta\kappa_e + \Delta\kappa_b \implies \Delta\kappa_e = \Delta\kappa_b \approx \frac{1}{2}\Delta\kappa, \tag{13}$$

obtaining

$$\delta n \approx \frac{\pi}{L_\kappa}\bar{\delta n}, \qquad \gamma \approx \frac{\pi}{L_\kappa}\bar{\gamma}, \tag{14}$$

Through which the coupling beat length is related to the corresponding physical parameters. Such relation is illustrated in Fig. 3 for a wide range of possible beat lengths. The approximation is validated numerically, determining that it introduces a relative error of $\approx 1\%$ on the total beat length.

Optics EXPRESS

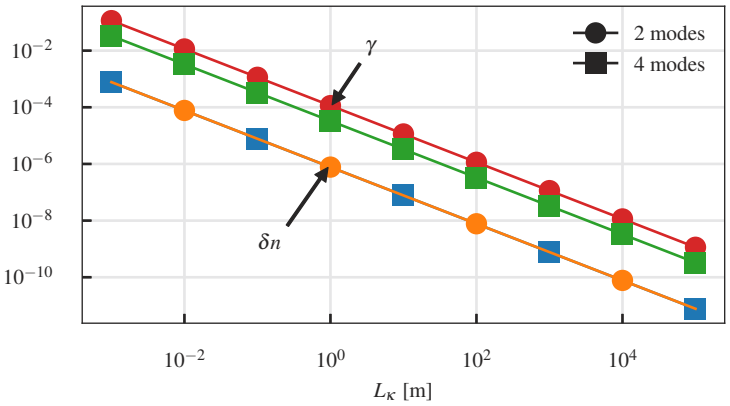

Fig. 3. Birefringence (orange and blue lines, indicated by δn) and core ellipticity (red and green lines, indicated by γ) for the two considered fibers and for a given coupling beat length L_κ. Circle (square) markers refer to the 2 (4) mode fiber.

4.2. Optimization of the nonlinear step

As shown in Ref. [2], due to symmetry properties, many of the overlap integrals $Q^{(i)}_{\nu\rho\mu\eta}$ are null. However, the mode distributions are computed with a FEM solver that introduces numerical errors. We tackle the issue of identifying which coefficients should be discarded by following the approach detailed in [2], setting a threshold coefficient ϵ, and only considering the nonlinear contributions whose overlap integrals satisfy

$$|Q^{(i)}_{\nu\rho\mu\eta}| > \epsilon \max_{\nu\rho\mu\eta} |Q^{(i)}_{\nu\rho\mu\eta}|, \qquad i \in 1, \ldots, 5. \tag{15}$$

Using $\epsilon = 0.01$, about 90 percent of the coefficients can be discarded, resulting in a significant acceleration of the integration algorithm. We ran a series of simulations to evaluate the effect of using this technique noting no significant changes between the results, confirming the viability of the approach.

4.3. Simulation results

Equations (1) were integrated for the two different fibers that have been previously introduced, aiming to understand how different levels of linear coupling can influence the statistics of the distributed amplifier's gain.

For the specified levels of perturbation length L_κ and correlation length L_c, we solve Eq. (1) for an ensemble of N_e different realizations of the process describing the orientation angle $\theta_k(z)$ of the perturbations acting on the fiber, obtaining the evolution of the vector of complex amplitudes $\mathbf{a}(z; \omega_s)$ for each realization.

Remembering the way in which the entries of $\mathbf{a}$ are organized, i.e. with alternating x- and y-polarizations of a mode, the total power in each spatial mode at the signal frequency ω_s is given by

$$P_\nu(z) = |a_{2\nu}(z)|^2 + |a_{2\nu+1}(z)|^2, \quad \nu \in [0, \ldots, N_s - 1], \tag{16}$$

where N_s is the number of spatial modes, which is equal to 3 for the 2-mode fiber and to 6 for the 4-mode fiber. The amplifier gain for mode ν is then computed for the kth realization of the

Optics EXPRESS

process $\theta_k(z)$ as

$$G_\nu(k) = \frac{P_\nu(L;\theta_k)}{P_\nu(0)}, \tag{17}$$

computing its ensemble mean as

$$\langle G_\nu \rangle = \frac{1}{N_e} \sum_{k=1}^{N_e} G_\nu(k). \tag{18}$$

From the same quantities, the signal power variance at the end of the amplifier can also be evaluated. With the Manakov approach used so far in the liturature, only the mode-averaged nonlinear effects are evaluated, while their statistics, which can be important to predict the variability among different fiber realizations or due to time-variant effects, are not considered. This aspect is particularly important for Raman amplifiers, which have been demonstrated to exhibit considerable gain fluctuations when PMD is present in SMFs [17,24].

To this end, we compute the variance of the signal power at the amplifier output as [17]

$$\sigma_\nu^2 = \frac{\langle P_\nu^2(L;\theta_k))\rangle}{\langle P_\nu(L;\theta_k)\rangle^2} - 1, \tag{19}$$

where $\langle\cdot\rangle$ indicates the mean over the ensemble of perturbation realizations, as in Eq. (18).

Regarding the simulation parameters, we set to 0 the coefficient σ related to Kerr effects, in order to focus only on Raman-related phenomena. The peak Raman gain coefficient was $g_R = 1\times10^{-13}$ mW^{-1}, and the corresponding values of the Raman response functions $\tilde{a}$ and $\tilde{b}$ were found following Ref. [28]. We consider no mode-dependent losses, and set the fiber loss coefficient to $\alpha_s = \alpha_p = 0.2$ dB km^{-1}; the integration step size is set to $\delta z = L_c/10$. The signals have an initial power of −40 dBm per spatial mode, while a total of 1 W is launched on the pump wavelength, equally distributed among the modes. The length of the simulated fibers is set to 50 km, which has been verified to be sufficient for the amplification dynamics to be fully exhausted for our simulation conditions.

The metrics in Eq. (18) and (19) are evaluated for two different initial conditions on the polarization of both pump and signal modes. In the first case, the polarization of each spatial mode at the fiber input for the signal frequency is set to be linear and parallel to that of the modes of the pump, while the second case considers orthogonal input polarizations between signal and pump modes.

4.3.1. 2-mode fiber

The ensemble average $\langle G_\nu \rangle$ for the 2-mode fiber is represented as a function of the perturbation beat length L_κ in Fig. 4. Correlation lengths of 10 m (left) and 100 m (right) are considered. The number of simulated fibers for each combination of parameters is $N_e = 5000$.

Let us remark that, as shown in Fig. 1, there is no linear mode coupling among LP_{01} and LP_{11} in this case and birefringence dominates. Focusing on the case L_c = 10m, we can clearly discern three regimes of propagation for the given fiber length, similarly to the case of randomly-birefringent SMFs [24]. For low degrees of birefringence, i.e. $L_\kappa \gg 1$ m, the mean gain is maximized on each mode for parallel input polarizations, reaching ≈ 41 dB for the LP_{11} modes, and ≈ 37 dB for the LP_{01} mode. With orthogonal input polarizations, the gain is instead minimized, almost totaling the link-losses of about −10 dB (it is not exactly equal because a small gain exists for orthogonally-polarized pumps too). In this regime, the only interaction between the three modes is determined by the nonlinear coupling. Pump and signal polarizations remain almost constant along the fiber due to the low values of coupling, explaining the observed behavior.

Optics EXPRESS

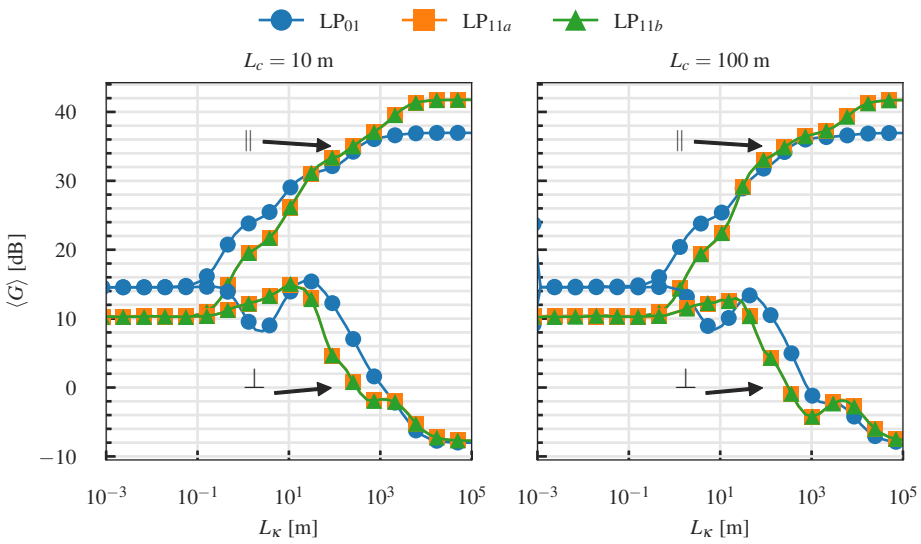

Fig. 4. Mean gain of the spatial modes of the 2-mode fiber as a function of the coupling beat length, for two values of the correlation length. The case when input signal and pump polarization are parallel (orthogonal) is indicated with ∥ (⊥).

For increasing birefringence and parallel input polarizations, the resulting average gain tends to decrease due to the polarization scrambling effect of linear coupling. It is interesting to note the presence of a few inflection points that are present in this regime for all three modes, although they are more accentuated for the case of the LP_{11} modes. For the case of orthogonal input polarizations the effect of linear coupling is beneficial to increase the average amplifier gain.

In the high-birefringence regime instead, for $L_\kappa \ll 1$ m, the alignment between pump and signal polarization is quickly lost due to the rapid exchange of power inside the group of degenerate modes, and the gain converges to the same average value both for the parallel and orthogonal input polarizations. The gain of both LP_{11a} and LP_{11b} modes is reduced to about 10 dB, resulting in the reduction of the equivalent gain by a factor of 4 (in dB), while the LP_{01} mode sees its average gain reduced to approximately 14 dB. Increasing the correlation length to 100 m, the dynamics remain are only slightly altered, but shifted toward longer beat length values.

At first sight it may seem that the Mode-Dependent-Gain (MDG) on modes of the LP_{11} group is zero for any value of birefringence.

Further insights can be gained by analyzing the signal power fluctuations through the evaluation of its standard deviation, given in Eq. (19). In Fig. 5, its value is represented as a percentage, and depicted for each mode as a function of the coupling beat length for the parallel (top left) and orthogonal (top right) polarization case, and for a correlation length of $L_c = 100$ m.

We can observe two different behaviors, depending on the modes we consider. For the LP_{01} mode, the three birefringence regimes previously highlighted are clearly observed. For large values of beat lengths, the signal fluctuations go to 0. On the other hand, for intermediate values of L_κ, two clearly defined peaks reaching a value of approximately 45% appear. This is consistent with the case of SMFs, albeit in the counterpumping configuration [17,24].

Regarding the LP_{11} group, a similar behavior is found for large beat lengths, where the signal fluctuations are negligible. For intermediate values of birefringence, the standard variation is fairly higher than the LP_{01} mode, reaching 70%, and showing a local maximum for much longer beat lengths. Additionally, in the high birefringence regime, the fluctuations do not decrease to 0 as for the LP_{01} mode, but instead remain constant at approximately 50%. This behavior can

Optics EXPRESS

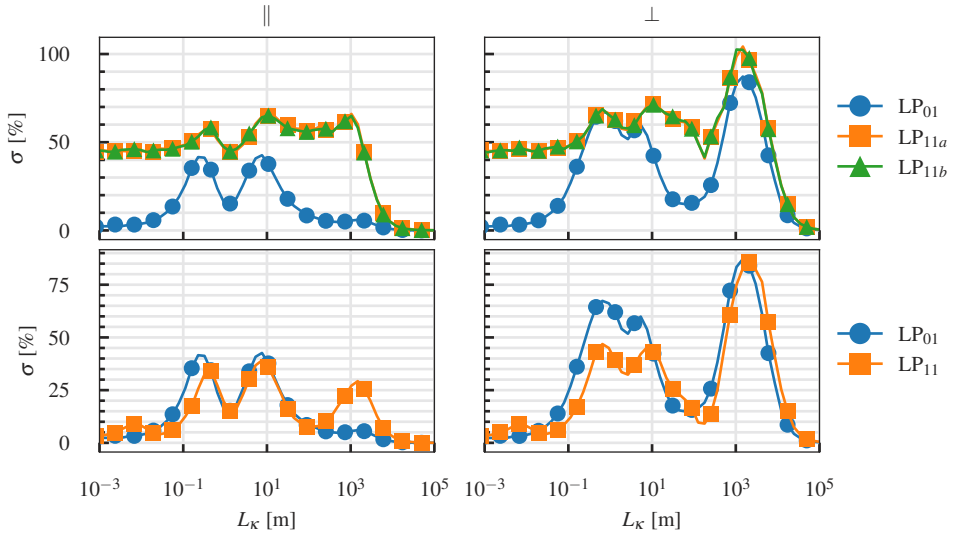

Fig. 5. Signal power variation of the gain of the 2-mode amplifier as a function of the coupling beat length, for L_c = 100m, for parallel (left column, ||) and orthogonal (right column, ⊥) input polarizations. Bottom row: power variation on the mode groups.

be intuitively explained by the fact that the LP_{11} group is 4-fold degenerate, meaning that the power exchange occurs both between polarizations and spatial modes. In order to verify this, we compute Eq. (19) on the total power contained in the LP_{11} group, and illustrate the results in the bottom graphs of Fig. 5. A similar behavior to that of the LP_{01} mode is now obtained, with the exception of a peak at approximately $L_\kappa = 10^3$ m. Interestingly, for this values of L_κ, a small increase in the signal variance is observed for the LP_{01} mode, which, in absence of inter-group coupling, can be explained by the Raman interaction between the two groups through the overlap integrals Q. The location of these peaks correspond to that of the inflection points observed in the behavior of the average gain, in Fig. 4. The same considerations can be made for the case of orthogonal input polarizations from the top right and bottom right graphs of Fig. 5, showing the same dynamics, although much more accentuated.

These results show that the gain equalization inside each mode group is only obtained on average, since random coupling caused by residual stress birefringence and core ellipticity of the fiber can make the power on each spatial mode fluctuate significantly for most of the realistic values of L_κ. In fact, with reference to Fig. 3 and Ref. [29], typical values of birefringence encountered for step-index SMFs, i.e. $10^{-8}<\delta n<10^{-6}$, correspond to a range of L_κ for which the signal power variation is as high as 40% (70%) for the parallel (orthogonal) input polarizations.

Moreover, the total power of the entire group only shows negligible fluctuations for really short beat lengths, which correspond to birefringence values that are typical of polarization-maintaining FMFs and therefore unrealistic for transmission fibers [30].

On the other side, observing Fig. 4 and 5 we can say that, for $L_\kappa > 10^4$ m, the power fluctuations induced by linear mode coupling are zero (even considering LP_{11a} and LP_{11b} separately). The same average gain of the modes belonging to the LP_{11} group is obtained in this regime because there are identical pumping conditions on the two modes and because the corresponding nonlinear coefficients Q are equal.

Optics EXPRESS

4.3.2. 4-mode fiber

When considering a fiber that supports 4 groups of LP modes, inter-group coupling is expected between the LP_{01}, LP_{02}, and LP_{21} groups, as a result of the perturbation tensor. Modes of the LP_{11} group instead only experiences intra-group coupling, meaning that similar behaviors to the 2-mode fiber are expected for this group. We employ the same simulation parameters of the previous section, but the analysis is shown only for the case L_c = 100m since similar results are obtained, provided that the perturbation beat length is properly scaled, as seen from the results for the 2-mode fiber.

The mean gain $\langle G_\nu \rangle$ is presented in Fig. 6 as a function of the beat length L_κ, considering linear parallel and orthogonal input polarizations between pump and signals.

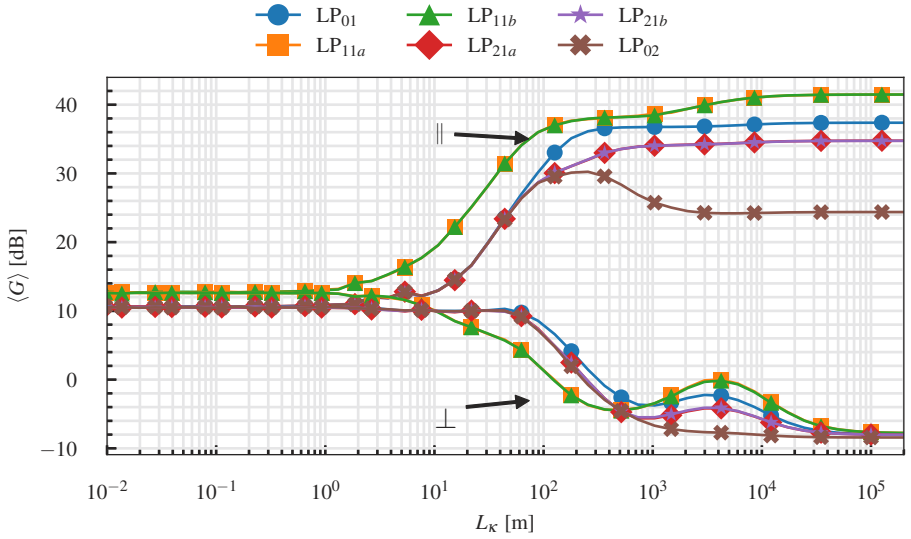

Fig. 6. Mean gain of the spatial modes of the 4-mode fiber as a function of the coupling beat length, for L_c = 100m. The case when input signal and pump polarization are parallel (orthogonal) is indicated with ∥ (⊥).

In the weak birefringence regime results are similar to the 2-mode fiber case. A mode-dependent gain is observed (due to different nonlinear overlap integrals). For parallel polarizations, the gain is maximized, with LP_{11} modes experiencing the highest amplification, approximately 42 dB, and the LP_{02} mode showing instead the smallest gain, 24 dB. LP_{01} and LP_{21} groups instead exhibit a maximum gain of 35 dB and 37 dB, respectively. For orthogonal input polarizations the gain is minimized, and equal to approximately −8 dB for each mode, showing a 2 dB reduction of the total link losses due to the weak contribution of the cross-polarized Raman response on the amplification process.

Decreasing the beat length, the effect of inter-group coupling can be readily observed for parallel polarizations; it is most apparent on the behavior of the average gain of the LP_{02} mode, which quickly merges with the curves for the LP_{21} modes for $L_\kappa \approx 10^2$ m. The LP_{01} average gain joins the aforementioned curves for $L_\kappa \approx 10^{1.5}$ m forming a "supergroup". This is in accordance with the computed coupling matrix for core-ellipticity in Fig. 2(b), where we can observe the slightly larger coupling coefficients between the LP_{02}-LP_{21} group pair with respect to the LP_{01}-LP_{21} combination. For values of birefringence $\delta_n \approx 10^{-7}$ typical for SMFs, corresponding to a beat length $L_\kappa \approx$ 10m in Fig. 3, the linear inter-group coupling is reached even when modest span lengths of 50 km are considered. When extrinsic perturbations such as twisting and bending, deriving mostly from cabling and installation, are considered, the effect of inter-group

Optics EXPRESS

coupling on the Raman gain is expected to be enhanced, and occur for shorter spans. Regarding the orthogonal polarizations case, the effect of inter-group coupling is similar, although the convergence between the LP_{21} and LP_{02} group pairs is reached for slightly longer beat lengths. The general behavior of reaching a local maximum gain for $L_\kappa \approx 10^{3.5}$ m observed in the 2-mode case is also present for all the modes except the LP_{02}, for which the increase is monotonic.

Finally, for high birefringence values corresponding to beat lengths L_κ<1 m, the curves for parallel and orthogonal polarizations converge to an average gain of 10 dB and 13 dB for the LP_{01}-LP_{21}-LP_{02} supergroup and the LP_{11} group, respectively.

As a general remark, modes belonging to groups with 4-fold degeneracy, i.e. LP_{11} and LP_{21}, maintain the same average gain for the entire interval of considered beat lengths, regardless of the relative orientation of pump and signal polarizations, similarly to the case of the 2-mode fiber.

The signal power fluctuations are evaluated for each mode with Eq. (19) and illustrated in Fig. 7 as a function of the beat length L_κ. The figure is organized similarly to the case of the 2-mode fiber, with the left and right columns corresponding to the parallel and orthogonal polarizations cases; the top row corresponds to the power fluctuation evaluated on each individual spatial mode, while the same metric computed on the total power of the LP_{11} and the LP_{01}-LP_{21}-LP_{02} supergroup is depicted in the bottom row.

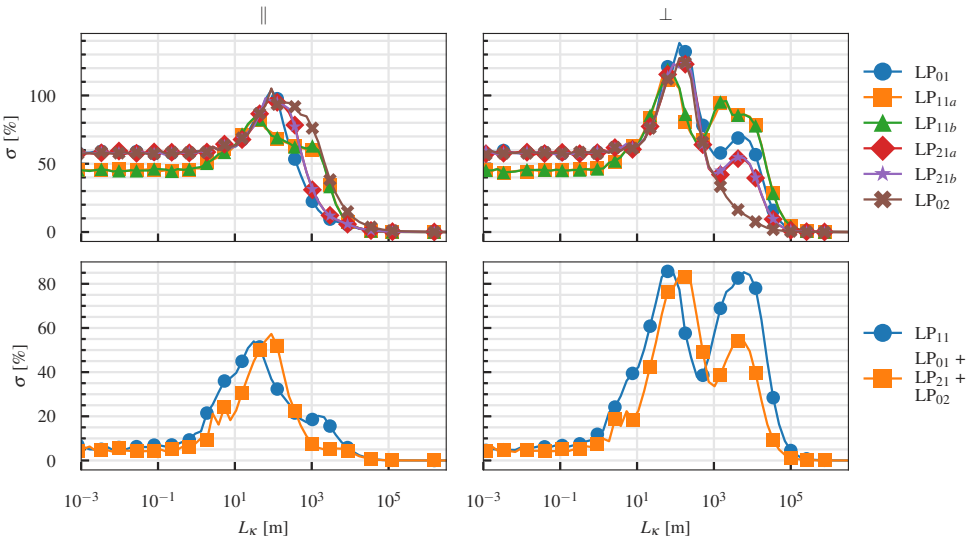

Fig. 7. Signal power variation of the 4-mode amplifier as a function of the coupling beat length, for L_c = 100 m, for parallel (left column, ∥) and orthogonal (right column, ⊥) input polarizations. Top row: power variation of the individual modes. Bottom row: power variation on the "supergroups".

For the parallel polarizations case, we can see that the signal power variation on each mode behaves similarly, presenting negligible fluctuations when the birefringence is unrealistically low (for L_κ>10^4 m). Decreasing the beat length, the variance quickly increases up to a maximum of 100% when $L_\kappa \approx 10^{1.5}$ m, i.e. when the LP_{01}-LP_{21}-LP_{02} supergroup is formed. Interestingly, even though no inter-group coupling affects the LP_{11} group, its variance is increased with respect to the 2-mode fiber case, which can be explained by the nonlinear coupling transferring the strong power fluctuations occurring between the modes forming the supergroup. For high birefringence, the power fluctuation stabilizes to about 50% for the LP_{11} mode, and to 55% for the modes that constitute the supergroup. In this case, the high power fluctuation so far exhibited only by the

Optics EXPRESS

4-fold degenerate LP_{11} group of the 2-modes fiber is also present for the 2-fold degenerate LP0, p groups of the 4-modes fiber, as a consequence of inter-group coupling.

If we consider the variance of the total power of the LP_{11} group and LP_{01}-LP_{21}-LP_{02} supergroup, the fluctuations decay for beat lengths $L_\kappa > 1$ m, as can be observed in the bottom-left graph of Fig. 7. The highest signal variation is still obtained at $L_\kappa \approx 10^{1.5}$ m for both supergroups, each reaching fluctuations of approximately 55%. Comparing these results with those obtained for the 2-mode fibers, we can notice the absence of multiple peaks; instead, a weak increase can be noticed at $L_\kappa \approx 10^3$ m for the LP_{11} group, where an inflection point is present in the corresponding gain curve in Fig. 6.

These effects are enhanced when considering orthogonal input polarizations, as seen in top- and bottom-right graphs of Fig. 7, where the peak we observed at $L_\kappa \approx 10^3$ m for parallel polarizations is much larger for modes belonging to both groups. Considering the variation on the individual spatial modes, the fluctuation increases with the average gain of the respective mode, as seen in Fig. 6.

5. Conclusions

In this article, a theoretical and numerical model that describes the propagation dynamics of the modes of a distributed Raman-amplified FMF links has been derived. Using analytical models published in the literature, the effect of stress birefringence and core ellipticity, intrinsic perturbations originating from the fiber manufacturing process, have been used to derive the linear coupling coefficients for FMFs supporting 2 and 4 groups of LP modes, respectively. The statistics of the amplification gain has been obtained by simulating thousands of realizations of the stochastic linear coupling process, described by the angle $\theta(z)$ along which the birefringence and core ellipticity perturbations are aligned.

For the 2-mode fiber, the considered perturbations induce coupling only among the quasi-degenerate modes belonging to the same LP group. Interaction between the two groups only occur through the nonlinear coupling coefficients that determine the Raman amplification process. Three coupling regimes are identified, similar to the results of SMF systems. When mode coupling is weak or negligible, the average gain on each mode is maximized (minimized) when signal and pump polarizations are parallel (orthogonal) at the fiber input, with the output signals showing no power fluctuations. As coupling increases, the average gain starts to decrease for parallel input polarizations (increase for orthogonal ones) and, more remarkably, the power variation on each mode group is very large. Finally, for large values of the perturbation strength, the average gain on each mode group for parallel and orthogonal input polarizations reach the same value. In this condition, the total power of each group of modes also shows reduced fluctuations.

When considering a FMF supporting the propagation of 4 groups of LP modes similar effects can be observed, with the addition of core ellipticity causing inter-group coupling between the LP_{01}, LP_{21}, and LP_{02} groups. For typical values of birefringence, the average gain of each mode belonging to this "supergroup" converges to the same value for a 50 km-long fiber. However, in this regime, high fluctuations of the signal power are observed.

In general, in the strong-coupling regime, the fluctuations of the total power of the group of coupled modes tends to zero, but the power on each spatial mode keeps exhibiting high variance, behaving similarly to the individual polarization components in a SMF system, in which PMD causes the Stokes vector of the fundamental mode to rotate on the Poincaré sphere and causing a rapid exchange of power between each orthogonal polarization states. Moreover, if the physical mechanism of coupling changes in time (e.g. due to fiber twist or bending) different super-groups can form and the gain behavior can be highly altered. Let us stress, though, that this regime is unlikely to be reached in a single span, with practical values of birefringence corresponding to

Optics EXPRESS

beat lengths in the order of tens of meters, becoming relevant only when considering long-haul multi-span transmissions.

Appendix: derivation of the propagation equations

When modeling nonlinear propagation effects in optical fibers, the starting point is to consider the third order nonlinear polarization of the material, which can be written as [17,25]

$$\mathbf{P}^{(3)}(\mathbf{r},t) = \frac{\epsilon_0}{2}\sigma[\mathbf{E}(\mathbf{r},t)\cdot\mathbf{E}(\mathbf{r},t)]\mathbf{E}(\mathbf{r},t) \tag{20a}$$

$$+\mathbf{E}(\mathbf{r},t)\int_0^\infty \epsilon_0 a(\tau)[\mathbf{E}(\mathbf{r},t-\tau)\cdot\mathbf{E}(\mathbf{r},t-\tau)]\,\mathrm{d}\tau \tag{20b}$$

$$+\mathbf{E}(\mathbf{r},t)\cdot\int_0^\infty \epsilon_0 b(\tau)[\mathbf{E}(\mathbf{r},t-\tau)\mathbf{E}(\mathbf{r},t-\tau)]\,\mathrm{d}\tau, \tag{20c}$$

where Eq. (20a) accounts for the instantaneous Kerr effect, while Eq. (20b) and Eq. (20c) describe the contribution of the parallel and cross-polarized delayed Raman responses $a(\tau)$ and $b(\tau)$.

By writing the total electric field and third order nonlinear polarization as the sum of signal and pump fields at frequencies ω_p and ω_s as

$$\mathbf{E} = \mathrm{Re}\big[\mathbf{E}_p\exp(-j\omega_p t) + \mathbf{E}_s\exp(-j\omega_s t)\big], \tag{21a}$$

$$\mathbf{P}^{(3)} = \mathrm{Re}\big[\mathbf{P}_p\exp(-j\omega_p t) + \mathbf{P}_s\exp(-j\omega_s t)\big], \tag{21b}$$

and inserting them in Eq. (20), the following expression is found [17]

$$\mathbf{P}_\ell^{(3)} = \mathbf{P}^{(3)}(\omega_\ell) = \frac{\epsilon_0}{8}[\sigma + 2\tilde{b}(0)](\mathbf{E}_\ell\cdot\mathbf{E}_\ell)\mathbf{E}_\ell^*(p_1\mathbf{N}_1) \tag{22a}$$

$$+\frac{\epsilon_0}{4}[\sigma + 2\tilde{a}(0) + \tilde{b}(0)](\mathbf{E}_\ell^*\cdot\mathbf{E}_\ell)\mathbf{E}_\ell(p_2\mathbf{N}_2) \tag{22b}$$

$$+\frac{\epsilon_0}{4}[\sigma + 2\tilde{a}(0) + \tilde{b}(\omega_\ell-\omega_f)](\mathbf{E}_f^*\cdot\mathbf{E}_f)\mathbf{E}_\ell(p_3\mathbf{N}_3) \tag{22c}$$

$$+\frac{\epsilon_0}{4}[\sigma + \tilde{b}(0) + \tilde{b}(\omega_\ell-\omega_f)](\mathbf{E}_f\cdot\mathbf{E}_\ell)\mathbf{E}_f^*(p_4\mathbf{N}_4) \tag{22d}$$

$$+\frac{\epsilon_0}{4}[\sigma + 2\tilde{a}(\omega_\ell-\omega_f) + \tilde{b}(0)](\mathbf{E}_f^*\cdot\mathbf{E}_\ell)\mathbf{E}_f(p_5\mathbf{N}_5), \tag{22e}$$

where the subscripts ℓ and f can can either be p or s to indicate pump or signal frequency, respectively. When $\ell = p$, then $f = s$, and vice versa. Inserting these expressions in the Maxwell equations, $\mathbf{E}_s$ and $\mathbf{E}_p$ are found to satisfy the nonlinear Helmholtz equation at their respective frequencies [17]

$$\nabla^2\mathbf{E}_\ell + \frac{\omega_\ell^2}{c^2}\boldsymbol{\epsilon}_\ell\mathbf{E}_\ell = -\frac{\omega_\ell^2}{\epsilon_0 c^2}\mathbf{P}_\ell. \tag{23}$$

In order to derive the equations for the case of a FMF, we can express the electric field as the sum of the individual modes supported by the fiber as follows

$$\mathbf{E}_\ell = \sum_{\mu=1}^{2M_\ell}\mathbf{F}_{\ell\mu}(x,y)A_{\ell\mu}(z)\exp(j\beta_{\ell\mu}z), \tag{24}$$

where M_ℓ is the number of spatial modes propagating at frequency ω_ℓ and the factor 2 accounts for polarization degeneracies; $\mathbf{F}_{\ell\mu}(x,y)$ is the mode function of mode μ at the frequency ω_ℓ, $A_{\ell\mu}$ is its complex amplitude, $\beta_{\ell\mu}$ is its propagation constant. From now on, the spatial dependence of

Optics EXPRESS

$\mathbf{F}_{\ell\mu}(x,y)$ and $A_{\ell\mu}(z)$ will be omitted for the sake of brevity. After substituting Eq. (24) in Eq. (23), using the slowly-varying envelope approximation [25], and collecting the $A_{\ell\mu}\exp(j\beta_{\ell\mu}z)$ terms, Eq. (23) becomes

$$\begin{aligned}\nabla^2\mathbf{E}_\ell + \frac{\omega_\ell^2}{c^2}\boldsymbol{\epsilon}_\ell\mathbf{E}_\ell = \sum_{\mu=1}^{2M_\ell} A_{\ell\mu}\left[\nabla_\perp^2\mathbf{F}_{\ell\mu} + \left(\frac{\omega_\ell^2}{c^2}\boldsymbol{\epsilon}_\ell - \beta_{\ell\mu}^2\right)\mathbf{F}_{\ell\mu}\right]\exp(j\beta_{\ell\mu}z)\\ + \sum_{\mu=1}^{2M_\ell}\mathbf{F}_{\ell\mu}2j\beta_{\ell\mu}\frac{\partial A_{\ell\mu}}{\partial z}\exp(j\beta_{\ell\mu}z) = -\frac{\omega_\ell^2}{\epsilon_0 c^2}\mathbf{P}_\ell,\end{aligned} \tag{25}$$

where we expressed the Laplacian operator as its transversal and longitudinal (with respect to the direction of propagation) components $\nabla^2 = \nabla_\perp^2 + \partial_z^2$.

To include the effect of linear coupling between the modes, a small perturbation to the permittivity tensor, describing the physical effects of the considered source of coupling, is applied [8,9]

$$\boldsymbol{\epsilon}_\ell = \epsilon_\ell + \Delta\boldsymbol{\epsilon}_\ell, \tag{26}$$

and Eq. (25) becomes

$$\begin{aligned}\sum_{\mu=1}^{2M_\ell} A_{\ell\mu}\left[\nabla_\perp^2\mathbf{F}_{\ell\mu} + \left(\frac{\omega_\ell^2}{c^2}\epsilon_\ell - \beta_{\ell\mu}^2\right)\mathbf{F}_{\ell\mu}\right]\exp(j\beta_{\ell\mu}z) + \sum_{\mu=1}^{2M_\ell}\frac{\omega_\ell^2}{c^2}\Delta\boldsymbol{\epsilon}_\ell\mathbf{F}_{\ell\mu}A_{\ell\mu}\exp(j\beta_{\ell\mu}z)\\ + \sum_{\mu=1}^{2M_\ell}\mathbf{F}_{\ell\mu}2j\beta_{\ell\mu}\frac{\partial A_{\ell\mu}}{\partial z}\exp(j\beta_{\ell\mu}z) = -\frac{\omega_\ell^2}{\epsilon_0 c^2}\mathbf{P}_\ell.\end{aligned} \tag{27}$$

The term in square brackets of the first term of Eq. (27) is the Helmholtz equation, which vanishes under the hypothesis of the mode distributions not being affected by nonlinearity, giving

$$\sum_{\mu=1}^{2M_\ell}\frac{\omega_\ell^2}{c^2}\Delta\boldsymbol{\epsilon}_\ell\mathbf{F}_{\ell\mu}A_{\ell\mu}\exp(j\beta_{\ell\mu}z) + \sum_{\mu=1}^{2M_\ell}\mathbf{F}_{\ell\mu}2j\beta_{\ell\mu}\frac{\partial A_{\ell\mu}}{\partial z}\exp(j\beta_{\ell\mu}z) = -\frac{\omega_\ell^2}{\epsilon_0 c^2}\mathbf{P}_\ell. \tag{28}$$

We then left-multiply by $\mathbf{F}_{\ell\nu}^\dagger$, integrate on the infinite transverse plane, and use the following orthogonality conditions, valid in the weakly guiding approximation [8]

$$\frac{\beta_{\ell\nu}}{2\omega_\ell\mu_0}\iint\mathbf{F}_{\ell\nu}^\dagger\mathbf{F}_{\ell\mu}\,\mathrm{d}x\mathrm{d}y = \delta_{\nu,\mu}, \tag{29}$$

to obtain the following equations

$$\sum_{\mu=1}^{2M_\ell}\frac{\omega_\ell^2}{c^2}A_{\ell\mu}\exp(j\beta_{\ell\mu}z)\iint_{-\infty}^{+\infty}\mathbf{F}_{\ell\nu}^\dagger\Delta\boldsymbol{\epsilon}_\ell\mathbf{F}_{\ell\mu}\,\mathrm{d}x\mathrm{d}y + 4j\omega_\ell\mu_0\frac{\partial A_{\ell\nu}}{\partial z}\exp(j\beta_{\ell\mu}z) = -\iint_{-\infty}^{+\infty}\mathbf{F}_{\ell\nu}^\dagger\frac{\omega_\ell^2}{\epsilon_0 c^2}\mathbf{P}_\ell\,\mathrm{d}x\mathrm{d}y. \tag{30}$$

Dividing by $4j\omega_\ell\mu_0$, introducing the following change of variables,

$$a_{\ell\mu} = A_{\ell\mu}\exp(j\beta_{\ell\mu}z), \tag{31a}$$

$$\frac{\partial A_{\ell\mu}}{\partial z} = \exp(-j\beta_{\ell\mu}z)\left(\frac{\partial a_{\ell\mu}}{\partial z} - j\beta_{\ell\mu}a_{\ell\mu}\right), \tag{31b}$$

and rearranging the terms, we can highlight the z-derivative of the mode amplitude obtaining

$$\frac{\partial a_{\ell\nu}}{\partial z} - j\beta_{\ell\nu}a_{\ell\nu} - j\sum_{\mu=1}^{2M_\ell}a_{\ell\mu}\frac{\omega_\ell}{4}\iint_{-\infty}^{+\infty}\mathbf{F}_{\ell\nu}^\dagger\epsilon_0\Delta\boldsymbol{\epsilon}_\ell\mathbf{F}_{\ell\mu}\,\mathrm{d}x\mathrm{d}y = \frac{j\omega_\ell}{4}\iint_{-\infty}^{+\infty}\mathbf{F}_{\ell\nu}^\dagger\mathbf{P}_\ell\,\mathrm{d}x\mathrm{d}y. \tag{32}$$

Optics EXPRESS

We now split the permittivity perturbation in its real and imaginary parts:

$$\Delta\boldsymbol{\epsilon}_\ell = \Delta\tilde{\boldsymbol{\epsilon}}_\ell - j\boldsymbol{\epsilon}''_{\boldsymbol{\ell}}. \tag{33}$$

The real part of the permittivity perturbation inside the summation in Eq. (32) defines the linear coupling coefficients as the overlap integral [8,9,19]

$$K_{\nu\mu}(\omega_\ell) = \epsilon_0 \frac{\omega_\ell}{4} \iint_{-\infty}^{+\infty} \mathbf{F}^\dagger_{\ell\nu} \Delta\tilde{\boldsymbol{\epsilon}}_\ell \mathbf{F}_{\ell\mu} \,\mathrm{d}x\mathrm{d}y. \tag{34}$$

The imaginary part instead defines the fiber losses. Assuming the absence of mode-dependent losses, and making use of Eq. (29), the corresponding summation in Eq. (32) is reduced to a single term reading

$$\frac{\omega_\ell}{4} \frac{2\omega_\ell \mu_0}{\beta_{\ell\nu}} \epsilon_0 \epsilon''_\ell a_{\ell\nu} \triangleq \frac{\alpha_\ell}{2} a_{\ell\nu}, \tag{35}$$

where α_ℓ is the power attenuation coefficient at frequency ℓ.

If we temporarily neglect the nonlinear polarization term, the linear propagation effects are finally completely described by the following equation,

$$\frac{\partial a_{\ell\nu}}{\partial z} = -\frac{\alpha_\ell}{2} a_\ell + j\beta_{\ell\nu} a_{\ell\nu} + j \sum_{\mu=1}^{2M_\ell} K_{\nu\mu}(\omega_\ell) a_{\ell\mu}. \tag{36}$$

Equation (36) can also be written in matrix form, describing the evolution of the vector $\mathbf{a}_\ell$ of complex mode amplitudes as

$$\frac{\partial \mathbf{a}_\ell}{\partial z} = -\frac{\alpha_\ell}{2} \mathbf{a}_\ell + j(\mathbf{B}_\ell + \mathbf{K}_\ell)\mathbf{a}_\ell, \tag{37}$$

where $\mathbf{B}_\ell$ is the diagonal matrix of propagation constants, and the elements of $\mathbf{K}_\ell$ are determined by Eq. (34), finding the results of [18] with the addition of fiber losses.

5.1. Nonlinear terms

Recalling the structure of the nonlinear polarization term in Eq. (22), the nonlinear terms on the right hand side of Eq. (32) can be written in a more compact form as

$$\frac{j\omega_\ell}{4} \sum_{i=1}^{5} p_i \iint_{-\infty}^{+\infty} \mathbf{F}^\dagger_{\ell\nu} \mathbf{N}_{i,\ell} \,\mathrm{d}x\mathrm{d}y. \tag{38}$$

Since all terms are similar in their structure, for the sake of brevity here we only show the derivation of the integral of the first term.

The computation of $\mathbf{N}_{1,\ell}$ starts by expanding the dot product of Eq. (22a), obtaining

$$\mathbf{E}_\ell \cdot \mathbf{E}_\ell = \left(\sum_{\mu=1}^{2M_\ell} \mathbf{F}_{\ell\mu} A_{\ell\mu} \exp\left(j\beta_{\ell\mu} z\right) \right) \cdot \left(\sum_{\eta=1}^{2M_\ell} \mathbf{F}_{\ell\eta} A_{\ell\eta} \exp\left(j\beta_{\ell\eta} z\right) \right) \tag{39}$$

$$= \sum_{\mu=1}^{2M_\ell} \sum_{\eta=1}^{2M_\ell} (\mathbf{F}_{\ell\mu} \cdot \mathbf{F}_{\ell\eta}) A_{\ell\mu} A_{\ell\eta} \exp\left[j(\beta_{\ell\mu} + \beta_{\ell\eta})z\right]. \tag{40}$$

Optics EXPRESS

Multiplying by $\mathbf{E}_\ell^*$ we can then write

$$\mathbf{N}_{1,\ell} = (\mathbf{E}_\ell \cdot \mathbf{E}_\ell)\mathbf{E}_\ell^* = \left(\sum_{\mu=1}^{2M_\ell}\sum_{\eta=1}^{2M_\ell}(\mathbf{F}_{\ell\mu}\cdot\mathbf{F}_{\ell\eta})A_{\ell\mu}A_{\ell\eta}\exp\left[j(\beta_{\ell\mu}+\beta_{\ell\eta})z\right]\right)\cdot\sum_{\rho=1}^{2M_\ell}\mathbf{F}_{\ell\rho}^*A_{\ell\rho}^*\exp\left(-j\beta_{\ell\rho}z\right) \tag{41}$$

$$= \sum_{\mu=1}^{2M_\ell}\sum_{\eta=1}^{2M_\ell}\sum_{\rho=1}^{2M_\ell}(\mathbf{F}_{\ell\mu}\cdot\mathbf{F}_{\ell\eta})\mathbf{F}_{\ell\rho}^*A_{\ell\mu}A_{\ell\eta}A_{\ell\rho}^*\exp\left[j(\beta_{\ell\mu}+\beta_{\ell\eta}-\beta_{\ell\rho})z\right] \tag{42}$$

$$= \sum_{\mu=1}^{2M_\ell}\sum_{\eta=1}^{2M_\ell}\sum_{\rho=1}^{2M_\ell}(\mathbf{F}_{\ell\mu}\cdot\mathbf{F}_{\ell\eta})\mathbf{F}_{\ell\rho}^*a_{\ell\mu}a_{\ell\eta}a_{\ell\rho}^*, \tag{43}$$

where in the last line we applied the change of variable defined by Eq. (31b).

Multiplying by $\mathbf{F}_{\ell\nu}^*$ and integrating on the transverse plane, we obtain the following

$$\iint_{-\infty}^{+\infty}\mathbf{F}_{\ell\nu}^\dagger\mathbf{N}_{1,\ell}\,\mathrm{d}x\mathrm{d}y = \sum_{\mu=1}^{2M_\ell}\sum_{\eta=1}^{2M_\ell}\sum_{\rho=1}^{2M_\ell}a_{\ell\mu}a_{\ell\eta}a_{\ell\rho}^*\iint_{-\infty}^{+\infty}(\mathbf{F}_{\ell\mu}\cdot\mathbf{F}_{\ell\eta})(\mathbf{F}_{\ell\rho}^*\cdot\mathbf{F}_{\ell\nu}^*)\,\mathrm{d}x\mathrm{d}y. \tag{44}$$

Rewriting the overlap integral as

$$Q_{\nu\rho\mu\eta}^{(1)}(\omega_\ell) = \iint_{-\infty}^{+\infty}(\mathbf{F}_{\ell\nu}^*\cdot\mathbf{F}_{\ell\rho}^*)(\mathbf{F}_{\ell\mu}\cdot\mathbf{F}_{\ell\eta})\,\mathrm{d}x\mathrm{d}y, \tag{45}$$

we then obtain the expression of the first nonlinear term for mode ν, which can be written as

$$\iint_{-\infty}^{+\infty}\mathbf{F}_{\ell\nu}^\dagger\mathbf{N}_{1,\ell}\,\mathrm{d}x\mathrm{d}y = \sum_{\mu=1}^{2M_\ell}\sum_{\eta=1}^{2M_\ell}\sum_{\rho=1}^{2M_\ell}Q_{\nu\rho\mu\eta}^{(1)}a_{\ell\mu}a_{\ell\eta}a_{\ell\rho}^*. \tag{46}$$

The other nonlinear terms are similar and the expression for their overlap integrals are summarized in Table 1. If the mode function of the modes with indices ρ, μ, or η is complex-conjugated inside the integral, then it must also be complex-conjugated in the triple summation when computing the total nonlinear contribution.

Regrouping the linear part of the equation with the nonlinear terms just described, the complete system of coupled nonlinear equations of Eq. (1) is finally obtained.

Funding. Università degli Studi di Padova (SEED - BIRD2020); Ministero dell'Istruzione, dell'Università e della Ricerca (Departments of Excellence"–law 498 232/2016, PRIN 2017HP5KH7_003 - FIRST).

Disclosures. The authors declare no conflicts of interest.

Data availability. Data underlying the results presented in this paper are not publicly available at this time but may be obtained from the authors upon reasonable request.

References

1. D. J. Richardson, J. M. Fini, and L. E. Nelson, "Space-division multiplexing in optical fibres," Nat. Photonics **7**(5), 354–362 (2013).
2. F. Poletti and P. Horak, "Description of ultrashort pulse propagation in multimode optical fibers," J. Opt. Soc. Am. B **25**(10), 1645 (2008).
3. M. Kolesik and J. V. Moloney, "Nonlinear optical pulse propagation simulation: From Maxwell's to unidirectional equations," Phys. Rev. E **70**(3), 036604 (2004).
4. A. Mecozzi, C. Antonelli, and M. Shtaif, "Nonlinear propagation in multi-mode fibers in the strong coupling regime," Opt. Express **20**(11), 11673 (2012).
5. D. Marcuse, C. Manyuk, and P. Wai, "Application of the Manakov-PMD equation to studies of signal propagation in optical fibers with randomly varying birefringence," J. Lightwave Technol. **15**(9), 1735–1746 (1997).

Optics EXPRESS

6. S. Mumtaz, R.-J. Essiambre, and G. P. Agrawal, "Nonlinear Propagation in Multimode and Multicore Fibers: Generalization of the Manakov Equations," J. Lightwave Technol. **31**(3), 398–406 (2013).
7. A. Mecozzi, C. Antonelli, and M. Shtaif, "Coupled Manakov equations in multimode fibers with strongly coupled groups of modes," Opt. Express **20**(21), 23436–23441 (2012).
8. L. Palmieri and A. Galtarossa, "Coupling Effects Among Degenerate Modes in Multimode Optical Fibers," IEEE Photonics J. **6**(6), 1–8 (2014).
9. L. Palmieri, "Coupling mechanism in multimode fibers," Proc. SPIE **9009**, 90090G (2014).
10. A. Trichili, M. Zghal, L. Palmieri, A. Galtarossa, and M. Santagiustina, "Statistical analysis of nonlinear coupling in a WDM system over a two mode fiber," Opt. Express **26**(6), 6602 (2018).
11. C. Antonelli, A. Mecozzi, and M. Shtaif, "Raman amplification in multimode fibers with random mode coupling," Opt. Lett. **38**(8), 1188 (2013).
12. G. Marcon, A. Galtarossa, L. Palmieri, and M. Santagiustina, "Model-Aware Deep Learning Method for Raman Amplification in Few-Mode Fibers," J. Lightwave Technol. **39**(5), 1371–1380 (2021).
13. Y. Chen, J. Du, Y. Huang, K. Xu, and Z. He, "Intelligent gain flattening in wavelength and space domain for FMF Raman amplification by machine learning based inverse design," Opt. Express **28**(8), 11911–11920 (2020).
14. J. Zhou, "An analytical approach for gain optimization in multimode fiber Raman amplifiers," Opt. Express **22**(18), 21393 (2014).
15. J. Li, J. Du, L. Ma, M.-J. Li, K. Xu, and Z. He, "Second-order few-mode Raman amplifier for mode-division multiplexed optical communication systems," Opt. Express **25**(2), 810 (2017).
16. D. E. Ceballos-Herrera, R. Gutierrez-Castrejon, and J. A. Alvarez-Chavez, "Stimulated Raman Scattering and Four-Wave Mixing Effects on Crosstalk of Multicore Fibers," IEEE Photonics Technol. Lett. **30**(1), 63–66 (2018).
17. Q. Lin and G. P. Agrawal, "Vector theory of stimulated Raman scattering and its application to fiber-based Raman amplifiers," J. Opt. Soc. Am. B **20**(8), 1616 (2003).
18. D. Marcuse, "Coupled-Mode Theory for Anisotropic Optical Waveguides," Bell Syst. Tech. J. **54**(6), 985–995 (1975).
19. G. Guerra, M. Lonardi, A. Galtarossa, L. A. Rusch, A. Bononi, and L. Palmieri, "Analysis of modal coupling due to birefringence and ellipticity in strongly guiding ring-core OAM fibers," Opt. Express **27**(6), 8308 (2019).
20. N. Imoto, N. Yoshizawa, J. Sakai, and H. Tsuchiya, "Birefringence in single-mode optical fiber due to elliptical core deformation and stress anisotropy," IEEE J. Quantum Electron. **16**(11), 1267–1271 (1980).
21. D. Chowdhury and D. Wilcox, "Comparison between optical fiber birefringence induced by stress anisotropy and geometric deformation," IEEE J. Sel. Top. Quantum Electron. **6**(2), 227–232 (2000).
22. P. K. A. Wai and C. R. Menyuk, "Polarization decorrelation in optical fibers with randomly varying birefringence," Opt. Lett. **19**(19), 1517 (1994).
23. S. Buch, S. Mumtaz, R.-J. Essiambre, A. M. Tulino, and G. P. Agrawal, "Averaged nonlinear equations for multimode fibers valid in all regimes of random linear coupling," Opt. Fiber Technol. **48**, 123–127 (2019).
24. A. Galtarossa, L. Palmieri, M. Santagiustina, and L. Ursini, "Polarized Backward Raman Amplification in Randomly Birefringent Fibers," J. Lightwave Technol. **24**(11), 4055–4063 (2006).
25. G. P. Agrawal, *Nonlinear Fiber Optics, Optics and Photonics* (Academic Press, San Diego, 2001), 3rd ed.
26. C. R. Menyuk and B. S. Marks, "Interaction of polarization mode dispersion and nonlinearity in optical fiber transmission systems," J. Lightwave Technol. **24**(7), 2806–2826 (2006).
27. B. Mukherjee, I. Tomkos, M. Tornatore, P. Winzer, and Y. Zhao, eds., *Springer Handbook of Optical Networks*, Springer Handbooks (Springer International Publishing, Cham, 2020).
28. S. Trillo and S. Wabnitz, "Parametric and Raman amplification in birefringent fibers," J. Opt. Soc. Am. B **9**(7), 1061 (1992).
29. A. Galtarossa, L. Palmieri, A. Pizzinat, M. Schiano, and T. Tambosso, "Measurement of Local Beat Length and Differential Group Delay in Installed Single-Mode Fibers," J. Lightwave Technol. **18**(10), 1389–1394 (2000).
30. L. Yu, J. Zhao, Q. Mo, and G. Li, "The beat-length of polarization-maintaining few-mode-fiber measurement based on polarized interference," in *2016 15th International Conference on Optical Communications and Networks (ICOCN)*, (2016), pp. 1–3.